IEICE TRANS. COMMUN., VOL.E98–B, NO.7 JULY 2015

PAPER

Accurate Coherent Change Detection Method Based on Pauli Decomposition for Fully Polarimetric SAR Imagery

Ryo OYAMA[†a)], ***Student Member***, **Shouhei KIDERA**[†], ***and*** **Tetsuo KIRIMOTO**[†], ***Members***

SUMMARY Microwave imaging techniques, particularly for synthetic aperture radar (SAR), produce high-resolution terrain surface images regardless of the weather conditions. Focusing on a feature of complex SAR images, coherent change detection (CCD) approaches have been developed in recent decades that can detect invisible changes in the same regions by applying phase interferometry to pairs of complex SAR images. On the other hand, various techniques of polarimetric SAR (PolSAR) image analysis have been developed, since fully polarimetric data often include valuable information that cannot be obtained from single polarimetric observations. According to this background, various coherent change detection methods based on fully polarimetric data have been proposed. However, the detection accuracies of these methods often degrade in low signal-to-noise ratio (SNR) situations due to the lower signal levels of cross-polarized components compared with those of co-polarized ones. To overcome the problem mentioned above, this paper proposes a novel CCD method by introducing the Pauli decomposition and the weighting of component with their respective SNR. The experimental data obtained in anechoic chamber show that the proposed method significantly enhances the performance of the receiver operation characteristic (ROC) compared with that obtained by a conventional approach.

key words: *synthetic aperture radar (SAR), fully polarimetric analysis, coherent change detection (CCD), pauli decomposition*

1. Introduction

Synthetic aperture radar (SAR) is one of the most useful tools for microwave remote sensing system as it can estimate the structure of terrain surface regardless lighting or weather conditions [1], [2]. As a notable feature of SAR image, we can obtain a complex-valued image, the phase information of which can include information on the height or structural features of targets. In focusing on this feature of SAR images, coherent change detection (CCD) techniques have been widely developed to detect slight surface changes using a phase rotation of the SAR image [3], [4]. The concept of CCD is simply based on a local spatial correlation between sequential complex SAR images obtained through observation of the same region at different times. There are various extensions of the original CCD method, such as more accurate change detection using the phase of the coherence function [5], or the height change estimation based on phase interferometry of the coherence function [6].

On the other hand, a polarimetric SAR(PolSAR) system has been actively investigated [7], [8], that utilizes a full combination of vertical and horizontal polarizations. Actually, there are various PolSAR techniques focusing on identification on terrain surface, such as the vegetation, forest or urban areas by decomposing the scattering matrix obtained by the fully polarimetric data. In recent years, the methods have attracted great attention since the PolSAR technique is useful for monitoring of natural disaster damage from such dangers as earthquakes, landslides or tsunami, by exploiting the high sensitivity of polarimetric data to changes of terrain surface [7]. For example, the literature [9] optimizes the coherence functions among full PolSAR images with a single observation to extract the target structures. Furthermore, the interferometry approaches using PolSAR images known an PolInSAR has been developed such as in [10], where the phase difference among PolSAR images is well eliminated by optimizing the coefficients for coherence functions of each PolSAR images.

Several CCD methods extended to fully polarimetric data have been developed, such as using a maximum likelihood estimation [11], or the log likelihood change statistic (LLCS) [12], where a probability density function of surface change is used as *a priori* information. As another approach of fully polarimetric oriented CCD without *a priori* information, *canonical correlation* based analysis has been proposed [13]. However, the detection accuracy of this method significantly degrades in cases where the SNR level for each PolSAR image is considerably different, because this method assesses each PolSAR image without discriminating the SNR level in calculating canonical correlation coefficients.

To obtain more accurate CCD performance using fully polarimetric data, this paper proposes a novel CCD index based on the Pauli decomposition of fully polarimetric SAR images and synthesizing the coherence function with SNR based weighting. The significant weighting of optimal component of the Pauli scattering vector that represent the changes improves the performance of the change detection. The experimental results, obtained in an anechoic chamber assuming a 1/100 scaled-down model of X-band radar, show that the proposed index significantly exceeds the ROC (Receiver Operating Characteristics) performance compared with that obtained with other single or fully polarimetric data synthesis methods.

This paper is organized as follows. In Sect. 2, the system model is introduced. Section 3 presents the conventional CCD method employing a fully polarimetric SAR image. Section 4 describes the principles and methods of the

Manuscript received November 28, 2014.
Manuscript revised March 2, 2015.

[†]The authors are with the Graduate School of Informatics and Engineering, The University of Electro-Communications, Chofu-shi, 182-8585 Japan.
a) E-mail: oyama@secure.ee.uec.ac.jp

DOI: 10.1587/transcom.E98.B.1390

proposed method exploiting the fully polarimetric SAR image based on a Pauli decomposition. Finally, the experimental results described in Section 5 demonstrate that the proposed method enhances ROC performance, compared with the conventional method, even in noisy situations.

2. System Model

Figure 1 shows the observation geometry. The target is assumed to have a rough surface around the $z = 0$ plane, and the propagation speed of the microwaves is a known constant. Monostatic radar is used to correct a set of scans along the line $z = \mathrm{z}_0$, $y = 0$ with transmitting and receiving antenna, located at $(x, 0, \mathrm{z}_0)$. The off-nadir angle is denoted by θ. Each antenna receives the complex-valued reflection signal $S(x; f)$ at each frequency f, where the signal is swept through a finite frequency range. The target surface can be changed between the first and second observations. The two linear polarizations are assumed to be vertical (denoted by V) and horizontal (denoted by H) with respect to the transmitting and receiving antennas. Then, fully polarimetric data characterized by VV, VH, HV, and HH are obtained (where HV denotes the vertical polarization in transmitted wave and horizontal polarization in received wave). The polarimetric SAR complex image, focused on the $z = 0$ plane at the p th observation, is defined as $s_p^{ab}(x, y)$, where a and b denote H or V, and p denotes 1 or 2. $s_p^{ab}(x, y)$ is obtained as a discretized SAR image. A scattering vector $\mathbf{X}_p$ is defined as

$$\boldsymbol{X}_p(x, y) = \left[\, s_p^{HH}(x, y),\ s_p^{HV}(x, y),\ s_p^{VV}(x, y) \,\right]^{\mathrm{T}}, \quad (1)$$
$(p = 1, 2)$.

The normal coherence function $\gamma(x, y)$ between the complex SAR images $s_1^{ab}(x, y)$ and $s_2^{ab}(x, y)$ is defined as [3]

$$\gamma(x, y) = \frac{\iint_{\Omega(x,y)} s_1^{ab}(x' - x, y' - y) \cdot \{s_2^{ab}(x' - x, y' - y)\}^* \mathrm{d}x'\mathrm{d}y'}{\sqrt{\iint_{\Omega(x,y)} \left|s_1^{ab}(x' - x, y' - y)\right|^2 \mathrm{d}x'\mathrm{d}y'} \sqrt{\iint_{\Omega(x,y)} \left|s_2^{ab}(x' - x, y' - y)\right|^2 \mathrm{d}x'\mathrm{d}y'}}, \quad (2)$$

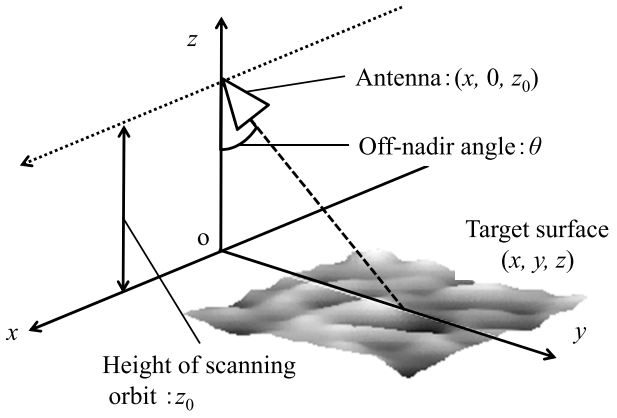

Fig. 1 Observation geometry.

where * denotes a complex conjugate and $\Omega(x, y)$ denotes the size of the correlation. Obviously, $0 \le |\gamma(x, y)| \le 1$ holds. The region (x, y) is regarded as the "changed" region, if $|\gamma(x, y)| \le \gamma_0$ is satisfied, where γ_0 is the threshold for the change detection. Otherwise, the regions are classified as being in the "unchanged" region.

3. Conventional Method

There are several CCD methods that can be extended to fully polarimetric data for more accurate change detection. As one of the most efficient methods, this section briefly introduces the method [13] that is based on a *canonical correlation* among the fully polarimetric SAR images. The *canonical correlation* is mostly used for analyzing correlative relationships among more than three variables. According to this, the literature [13] introduces the change detection index γ_{conv} as the maximum eigenvalue of the canonical correlation matrix, as $\boldsymbol{S}_{11}^{-1}\boldsymbol{S}_{12}\boldsymbol{S}_{22}^{-1}\boldsymbol{S}_{12}^{*T}$. Here, $\boldsymbol{S}_{11}$, $\boldsymbol{S}_{22}$ and $\boldsymbol{S}_{12}$ are defined as

$$\boldsymbol{S}_{uv} = \boldsymbol{X}_u(x, y)\, \boldsymbol{X}_v(x, y)^{*T}, \quad (3)$$

where $u, v = 1, 2$ denotes the number of observations. Each eigenvalue of the canonical correlation matrix $\boldsymbol{S}_{11}^{-1}\boldsymbol{S}_{12}\boldsymbol{S}_{22}^{-1}\boldsymbol{S}_{12}^{*T}$ provides a correlation coefficient between the two observations.

Although the effectiveness of this method has been verified in literature [13], it is predicted that this method suffers from accuracy degradation in regard to change detection, when the SNR level of each PolSAR image is considerably different. This is because each PolSAR image is equivalently assessed by calculating a *canonical correlation*.

4. Proposed Method

As a solution for the problem described in the previous section, this paper introduces a novel CCD index using Pauli decomposition and the synthesis of each PolSAR image weighted by its SNR level. Pauli decomposition has been proven effective for identifying the structure of a terrain surface, such as artificial buildings, cultivated field or forest areas [14]. The scattering matrix obtained from a fully polarimetric observation can be decomposed by the following Pauli matrices

$$\begin{bmatrix} s_p^{HH}(x, y) & s_p^{HV}(x, y) \\ s_p^{VH}(x, y) & s_p^{VV}(x, y) \end{bmatrix} = k_{p,1}(x, y) \begin{bmatrix} 1 & 0 \\ 0 & 1 \end{bmatrix} + k_{p,2}(x, y) \begin{bmatrix} 1 & 0 \\ 0 & -1 \end{bmatrix} + k_{p,3}(x, y) \begin{bmatrix} 0 & 1 \\ 1 & 0 \end{bmatrix}, \quad (4)$$

where $k_{p,i}(x, y)$ $(i = 1, 2, 3)$ denotes a complex-valued coefficient. The Pauli scattering vector $\boldsymbol{k}_p(x, y)$ is calculated as

$$\boldsymbol{k}_p(x,y) = \sqrt{2}\begin{bmatrix} k_{p,1}(x,y) \\ k_{p,2}(x,y) \\ k_{p,3}(x,y) \end{bmatrix} = \frac{1}{\sqrt{2}}\begin{bmatrix} s_p^{HH}(x,y) + s_p^{VV}(x,y) \\ s_p^{HH}(x,y) - s_p^{VV}(x,y) \\ 2s_p^{HV}(x,y) \end{bmatrix}. \tag{5}$$

In Eq. (5), the first, second and third rows of the Pauli vector $\boldsymbol{k}_p(x,y)$ are regarded as the surface, double and volume scattering components, respectively. To consider the SNR imbalance of each Pauli components, a weighted Pauli scattering vector $\boldsymbol{f}_p(x,y)$ is defined as

$$\boldsymbol{f}_p(x,y) \equiv \boldsymbol{w}_p(x,y)\,\boldsymbol{k}_p(x,y) \quad (p = 1,2), \tag{6}$$

where $\boldsymbol{w}_p(x,y)$ denotes the weighting matrix as

$$\boldsymbol{w}_p(x,y) = \frac{\mathrm{diag}\left(\mathrm{SNR}_{p,1}(x,y), \mathrm{SNR}_{p,2}(x,y), \mathrm{SNR}_{p,3}(x,y)\right)}{\sum_{i=1}^{3} \mathrm{SNR}_{p,i}(x,y)}, \tag{7}$$

where the subscript i denotes the row number of $\boldsymbol{k}_p$. Using $\boldsymbol{f}_p(x,y)$, the proposed method introduces a novel index as

$$\gamma_{\mathrm{pro}}(x,y) = \frac{\iint_{\Omega(x,y)} \boldsymbol{f}_1(x'-x,y'-y)^{*T} \cdot \boldsymbol{f}_2(x'-x,y'-y)\,\mathrm{d}x'\mathrm{d}y'}{\sqrt{\iint_{\Omega(x,y)} \left\|\boldsymbol{f}_1(x'-x,y'-y)\right\|^2 \mathrm{d}x'\mathrm{d}y'} \sqrt{\iint_{\Omega(x,y)} \left\|\boldsymbol{f}_2(x'-x,y'-y)\right\|^2 \mathrm{d}x'\mathrm{d}y'}}. \tag{8}$$

Here, $\mathrm{SNR}_{p,i}(x,y)$ is the local SNR around the correlation area $\Omega(x,y)$ for each Pauli component, and is defined as

$$\mathrm{SNR}_{p,i}(x,y) = \frac{E[|\boldsymbol{k}_{p,i}|^2]}{E[|\boldsymbol{n}_{p,i}|^2]}, \tag{9}$$

where $E[|\boldsymbol{k}_{p,i}|^2]$ denotes the space average of $|\boldsymbol{k}_{p,i}|^2$ in the correlation area $\Omega(x,y)$ introduced in Eq. (2). In addition, $\boldsymbol{n}_{p,i}$ denotes i th Pauli component at the image area focused by the received signals not including a reflection echo from a target (e.g. a propagation signal in co-axial cable). The proposed index considers the SNR balance in calculating the coherence function.

The actual procedure of the proposed method is summarized as follows.

Step 1)
Pauli scattering vectors $\boldsymbol{k}_1(x,y)$ and $\boldsymbol{k}_2(x,y)$ are obtained by decomposing the fully polarimetric SAR data.

Step 2)
$\boldsymbol{w}_1(x,y)$ and $\boldsymbol{w}_2(x,y)$ are calculated using Eq. (7) with the Pauli scattering vector and each SNR.

Step 3)
$\gamma_{\mathrm{pro}}(x,y)$ is calculated using Eq. (8).

Step 4)
If $\gamma_{\mathrm{pro}}(x,y) \le \gamma_0$, then the region (x,y) is regarded as the "changed" region, where γ_0 is the threshold for change detection. Otherwise, the region is classified as the "unchanged" region.

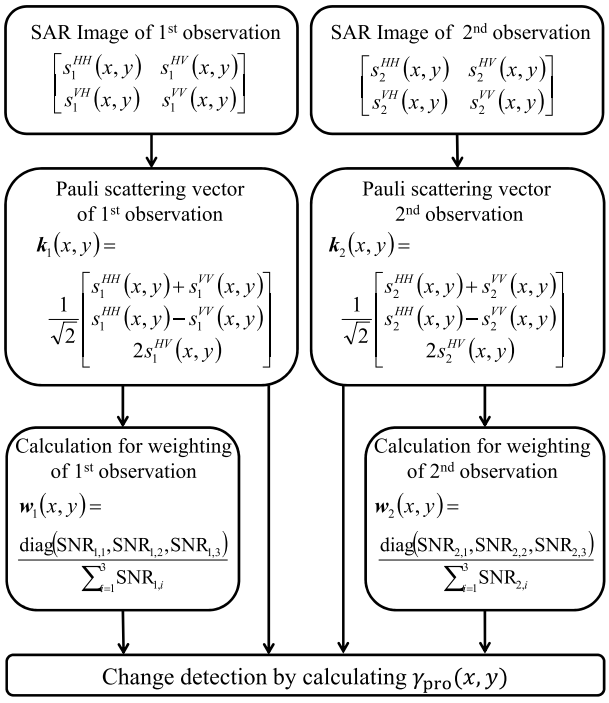

Fig. 2 Flowchart of the proposed method.

Figure 2 shows the flowchart of the proposed method.

5. Performance Evaluation with Experimental Data

This section presents a performance evaluation for the experiment. Here, we assume a 1/100 scale model for the observation geometry and spatial resolution, except at the center frequency, where the X-band radar system is assumed. Figure 3 shows the experimental geometry. The radio wave absorbers are embedded under a planar expanded polystyrene floor. To simulate the terrain surface, two clay targets shown in Fig. 4 are used. The width, depth and thickness of each clay target are 4.0×10^2 mm, 5.0×10^2 mm and 1.0×10^2 mm, respectively. To model the surface changes between twice observations, the tracks of a small tire are added to the right half of the target surface ($x \ge 0$), where the tracks are etched into the surface to a depth of 2 mm. Since these surface changes are quite small, the left and right photos in Fig. 4 offers apparently same view. The antenna scans at $-8.0 \times 10^2\,\mathrm{mm} \le x \le 8.0 \times 10^2\,\mathrm{mm}$, $y = 0\,\mathrm{mm}$, $z_0 = 1.0 \times 10^3\,\mathrm{mm}$. The minimum and maximum frequencies are $f_{\min} = 26\,\mathrm{GHz}$ and $f_{\max} = 40\,\mathrm{GHz}$. A vector network analyzer sweeps this frequency range with a 0.01 GHz interval. The off-nadir angle is 50.0 degree. The theoretical range and azimuth resolutions are 10.7 mm and 12.5 mm, respectively. Here, each correlation size $\Omega(x,y)$ of the conventional coherence index based on canonical correlation

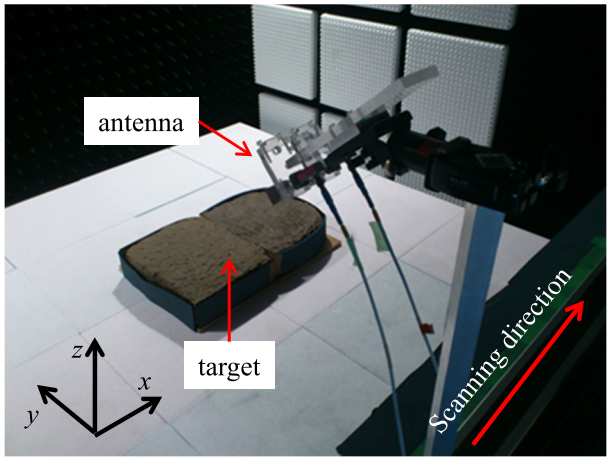

Fig. 3 Experimental geometry.

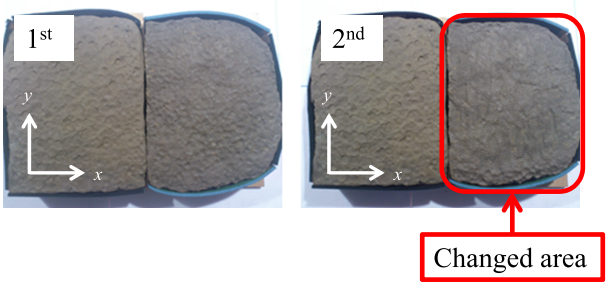

Fig. 4 Clay target (left: 1st observation, right:2nd observation).

defined by Eq. (2) and the proposed coherence defined by Eq. (8) is set to be three times larger than the spatial resolution of the SAR image. *HH*, *HV* and *VV* polarization data are acquired for each observation.

The left and right hand sides of Fig. 5 show the first and second observed SAR images in each polarization or Pauli decomposition image, respectively. The average SNRs defined in Eq. (9) for *HH*, *HV* and *VV* polarized SAR images are 24 dB, 7 dB and 23 dB, respectively. (a), (b) and (c) of Fig. 5 indicate that the intensity of $s^{HV}(x,y)$ is significantly less than that of $s^{HH}(x,y)$ and $s^{VV}(x,y)$. In addition, it is confirmed from (d), (e) and (f) of Figure 5 that only the 1st component of the Pauli decomposition, mainly contributing surface scattering, is emphasized. This indicates that the antenna mainly receives the scattering echo from the target surface. Figure 6 illustrates the distribution of the norm of coherence functions of the *canonical correlation* based conventional method $\left|\gamma_{\mathrm{conv}}(x,y)\right|$ and the proposed method $\left|\gamma_{\mathrm{pro}}(x,y)\right|$, respectively. While the norm of the coherent function of both methods falls below 1, the proposed method emphasizes the changed region by lowering the coherent function compared with that obtained by the conventional method.

To evaluate the accuracy of the change detection quantitatively, the receiver operating characteristic (ROC) is evaluated for each detection index. Here, the ROC denotes the relationship between the change detection probability and

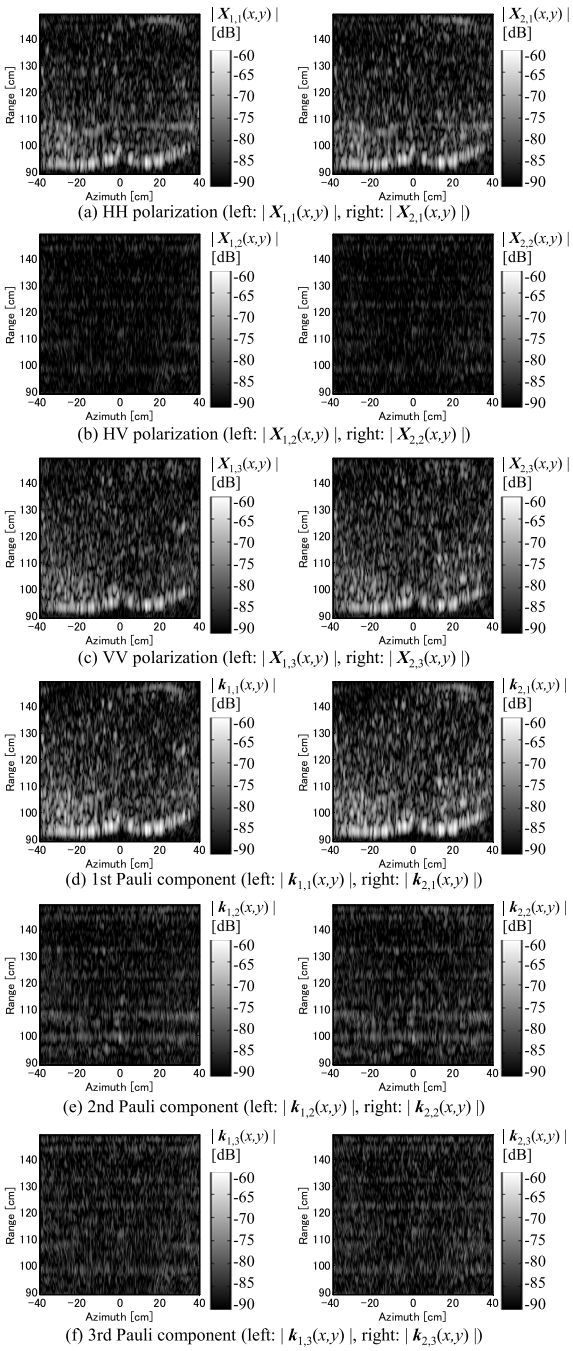

Fig. 5 Intensity of SAR images (left: 1st observation right: 2nd observation).

the false alarm rate, which is calculated by changing the detection threshold. The detection probability is denoted by $\mathrm{P_D}$, that the coherence value at changed area is below the threshold γ_0. The false-alarm rate is denoted by $\mathrm{P_{FA}}$, that the coherence value at unchanged area is below the threshold γ_0. Figure 7 shows the ROC for each synthesizing approach. $\left|\gamma_{\mathrm{HH}}\right|$, $\left|\gamma_{\mathrm{HV}}\right|$ and $\left|\gamma_{\mathrm{VV}}\right|$ denote the norm of the coherence functions calculated with single *HH*, *HV* and *VV* polarized SAR images, respectively. $\left|\gamma_{\mathrm{S}}\right|$, $\left|\gamma_{\mathrm{D}}\right|$ and $\left|\gamma_{\mathrm{V}}\right|$ correspond to the norms of coherence functions calculated with each component of the Pauli vector as $\boldsymbol{k}_{p,1}$, $\boldsymbol{k}_{p,2}$ and $\boldsymbol{k}_{p,3}$, re-

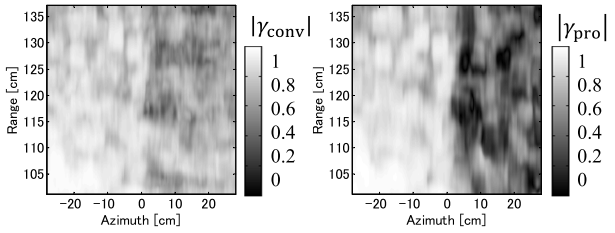

Fig. 6 Spatial distribution of norm of coherence index for each method. (left: the canonical correlation based method, right: the proposed method).

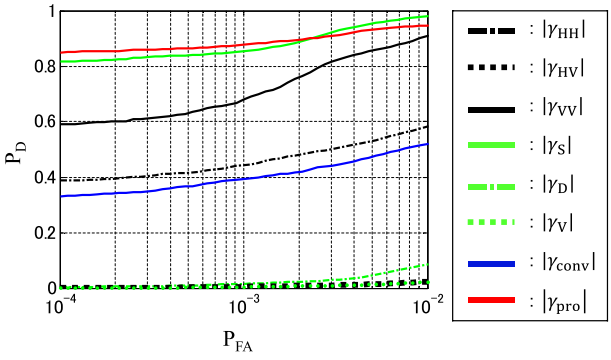

Fig. 7 ROC for each detection index.

spectively. Here, the ROC of single HV denoted as $|\gamma_{HV}|$ is exactly same as that of $|\gamma_V|$, because both components including only the HV component. $|\gamma_{conv}|$ and $|\gamma_{pro}|$ denote the *canonical correlation* based on the conventional method and the proposed method as in Eq. (8), respectively. This figure indicates that the proposed method, when compared with conventional method, enhances the ROC evaluation. This result is mainly because the proposed method emphasizes the scattering characteristics of the target by introducing the Pauli scattering vector, and reduces the effect of components that are sensitive to noise by weighting based on the SNR level. Furthermore, since the conventional method in [13] equivalently assesses the HH, VV and HV in calculating the canonical correlation, the ROC of the conventional method degrades compared with that obtained by HH, VV or the proposed method which include higher SNR components. However, some part of the ROC of the proposed method is inferior to that of $|\gamma_S|$, namely, only using surface scattering. This is because the proposed index is slightly dependent on the double and volume scattering components, even though the surface scattering strongly dominates in this target case.

Next, to investigate the validity of introducing the Pauli scattering vectors and weighting based on SNR, we investigate the ROC as shown in Fig. 8. In this figure, the red dashed line corresponds to the coherence function index using the Pauli decomposed components in Eq. (8) without the SNR weighting. The black solid line denotes the index where the scattering vector $\boldsymbol{X}'_p$ is used instead of $\boldsymbol{k}_p$ in Eq. (8). Here, $\boldsymbol{X}'_p$ is defined as

$$\boldsymbol{X}'_p(x,y) = \left[\, s_p^{HH}(x,y),\quad \sqrt{2}s_p^{HV}(x,y),\quad s_p^{VV}(x,y)\,\right]^{\mathrm{T}}. \tag{10}$$

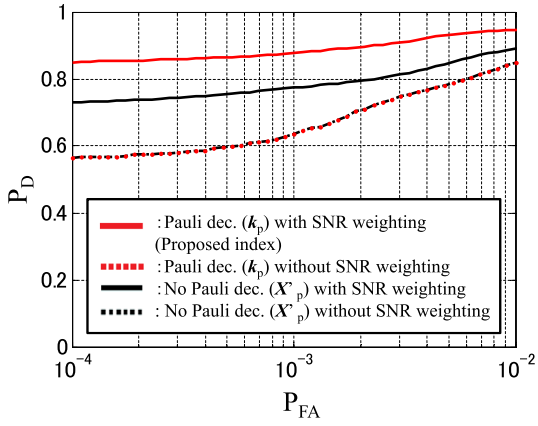

Fig. 8 ROC for investigating the validity of introducing Pauli scattering vector and weighting.

Note that, the norm of Eq. (10) is equal to that of Eq. (5). The black dashed line denotes the ROC when using $\boldsymbol{X}'_p$ instead of $\boldsymbol{k}_p$ but not using the SNR weighting. Figure 8 shows that the SNR weighting brings us more beneficial effect in ROC evaluation for both vectors $\boldsymbol{X}'_p$ and $\boldsymbol{k}_p$. Furthermore, the proposed index is more effective than using $\boldsymbol{X}'_p$ with a SNR weighting. This is because the proposed index based on Pauli decomposition considerably reduces the effect of unnecessary component for change detection. Actually, in this case, the first Pauli component, namely, surface scattering component is dominant. Thus, for the change detection, other components, such as double scattering or volume scattering are not needed for consideration. The proposed index can emphasize the SAR images generated by most dominant scattering component, and achieves more higher change detection performance compared with the simple synthesizing index as in Eq. (10), each component of which is not decomposed to actual scattering component.

6. Conclusions

This paper introduces a new change detection method for extracting fully polarimetric information to the maximum extent. As an essential solution for the conventional index-based canonical correlation, the proposed method employs Pauli decomposition and weighting based on the SNR for each SAR image. Experimental data gathered in an anechoic chamber have verified that the proposed method significantly enhances the ROC (receiver operating characteristic) compared to the conventional index or other possible combination indexes.

References

[1] W.M. Brown, "Synthetic aperture radar," IEEE Trans. Aerosp. Electron. Syst., vol.AES-3, no.2, pp.217–229, March, 1967.
[2] L.M.H. Ulander, H. Hellsten, and G. Stenstrom, "Synthetic-aperture radar processing using fast factorized back-projection," IEEE Trans. Aerosp. Electron. Syst., vol.39, no.3, pp.760–776, July 2003.

[3] R. Touzi, A. Lopes, J. Bruniquel, and P.W. Vachon, "Coherence estimation for SAR imagery," IEEE Trans. Geosci. Remote Sens., vol.37, no.1, pp.135–149, Jan. 1999.
[4] G. Franceschetti and R. Lanari, Synthetic Aperture Radar Processing, pp.185–195, CRC Press, New York, 1999.
[5] T. Hoshino, S. Kidera, and T. Kirimoto, "Accurate surface change detection method using phase of coherence function on SAR imagery," IEICE Trans. Commun., vol.E95-B, no.1, pp.263–270, Jan. 2012.
[6] R. Nakamata, S. Kidera, and T. Kirimoto, "Experimental study on accurate height change estimation method based on phase interferometry of band-divided SAR images," Proc. of 2013 IEEE Geoscience and Remote Sensing Symposium, IGARSS 2013, pp.620–623, Sept. 2013.
[7] Y. Yamaguchi, "Disaster monitoring by fully polarimetric SAR data acquired with ALOS-PALSAR," Proc. IEEE, vol.100, no.10, pp.2851–2860, Oct. 2012.
[8] T. Moriyama, S. Uratsuka, T. Umehara, M. Satake, A. Nadai, H. Maeno, K. Nakamura, Y. Yamaguchi, "A study on extraction of urban areas from polarimetric synthetic aperture radar image," Proc. Geosci.& Remote Sensing IGRASS'04, vol.1, pp.703–706, Sept. 2004.
[9] A. Marino, S.R. Cloude, and I.H. Woodhouse, "A polarimetric target detector using the Huynen Fork," IEEE Trans. Geosci. Remote Sens., vol.48, no.5, pp.2357–2366, 2010.
[10] S.R. Cloude and K.P. Papathanassiou, "Polarimetric SAR interferometry," IEEE Trans. Geosci. Remote Sens., vol.36, no.5, pp.1551–1565, Sept. 1998.
[11] L.M. Novak, "Coherent change detection for multi-polarization SAR," Proc. 39th Asilomar Conferenceon Signals, Systems and Computers, pp.568–573, 2005.
[12] A.S. Goh, M. Preiss, N.J.S. Stacy, and D.A. Gray, "The ingara bistatic SAR upgrade: First results," 2008 7th, European Conference on Synthetic Aperture Radar (EUSAR), pp.329–334, June 2008.
[13] R. Sharma, "Coherent change detection statistics for multiple polarization SAR images," Conference Record of the Forty-First Asilomar Conference on Signals, Systems and Computers, pp.2209–2212, Nov. 2007.
[14] X. Fabregas, A. Broquetas, J. Romeu, and L. Jofre, "Monostatic polarimetric calibration via target spinor," 1994 IEEE Geoscience and Remote Sensing Symposium IGARSS 1994, vol.3, pp.1374–1376, Aug. 1994

Ryo Oyama received his B.E. degrees in Electronic Engineering from University of Electro-Communications in 2013. He is currently studying M.E degree at the Graduate School of Informatics and Engineering, University of Electro-Communications. His current research interest is advanced radar signal processing of SAR application.

Shouhei Kidera received his B.E. degree in Electrical and Electronic Engineering from Kyoto University in 2003 and M.I. and Ph.D. degrees in Informatics from Kyoto University in 2005 and 2007, respectively. He is currently an Associate Professor in Graduate School of Informatics and Engineering, the University of Electro-Communications, Japan. His current research interest is in advanced radar signal processing or electromagnetic inverse scattering issue for ultra wideband (UWB) sensor. He was awarded Ando Incentive Prize fo the Study of Electronics in 2012, Young Scientist's Prize in 2013 by the Japanese Minister of Education, Culture, Sports, Science and Technology (MEXT), and Funai Achievement Award in 2014. He is a member of the Institute of Electrical and Electronics Engineering (IEEE) and the Institute of Electrical Engineering of Japan (IEEJ).

Tetsuo Kirimoto received the B.S. and M.S. and Ph.D. degrees in Communication Engineering from Osaka University in 1976, 1978 and 1995, respectively. During 1978–2003 he stayed in Mitsubishi Electric Corp. to study radar signal processing. From 1982 to 1983, he stayed as a visiting scientist at the Remote Sensing Laboratory of the University of Kansas. From 2003 to 2007, he joined the University of Kitakyushu as a Professor. Since 2007, he has been with the University of Electro-Communications, where he is a Professor at the Graduate School of Informatics and Engineering. His current study interests include digital signal processing and its application to various sensor systems. Prof. Kirimoto is a senior member of IEEE and a member of SICE (The Society of Instrument and Control Engineers) of Japan.